Available online at www.sciencedirect.com
SCIENCE DIRECT®
Polymer 44 (2003) 3883–3890
polymer
www.elsevier.com/locate/polymer

Surface chemical and morphological properties of a blend containing semi-crystalline and amorphous polymers studied with ToF-SIMS, XPS and AFM

Yu-Guo Lei[a], Zhuo-Lin Cheung[a], Kai-Mo Ng[b], Lin Li[c,*], Lu-Tao Weng[d], Chi-Ming Chan[a,*]

[a]*Department of Chemical Engineering, Hong Kong University of Science and Technology, Clear Water Bay, Hong Kong*
[b]*Advanced Engineering Materials Facility, Hong Kong University of Science and Technology, Clear Water Bay, Hong Kong*
[c]*State Key Laboratory of Polymer Physics and Chemistry, Center for Molecular Science, Institute of Chemistry, Chinese Academy of Sciences, Beijing 100080, China*
[d]*Materials Characterization and Preparation Facility, Hong Kong University of Science and Technology, Clear Water Bay, Hong Kong*

Received 17 September 2002; received in revised form 20 March 2003; accepted 18 April 2003

Abstract

The polymers BA-C8 and 6FBA-C8 were obtained by condensation polymerization of 1,8-dibromo-octane with bisphenol A and 4,4′-(hexafluoroisopropylidene)diphenol, respectively. A blend (BA-C8/6FBA-C8 (80/20)) containing 80 wt% of BA-C8 and 20 wt% 6FBA-C8 was prepared. Only one glass transition temperature was detected using a differential scanning calorimeter, suggesting that the blend is miscible. The surface chemical and morphological properties of the blend were studied as BA-C8 crystallized using atomic force microscopy, X-ray photoelectron spectroscopy, time-of-flight secondary ion mass spectrometry and contact angle measurements. The results of the surface analyses showed that the surface of the blend was found to be enriched in the 6FBA-C8 polymer, especially at the crystalline regions. The crystalline regions were found to be raised above the amorphous regions. Surface segregation and crystallization were the two main factors that contributed to the changes in the chemical composition and morphology of the surface.

Keywords: Semi-crystalline polymer blend; Surface morphology and chemical composition; Surface segregation

1. Introduction

The surface properties of materials are usually different from those of the bulk because the surface atoms and molecules experience a different environment compared to those in the bulk [1–3]. The properties of the topmost surface layer such as adhesion, wettability, biocompatibility, friction and chemical and catalytic activities are often important to many applications. Few studies have been performed on the surface chemical and morphological changes of polymer blends comprising both crystalline and amorphous components.

Studies have shown that the bulk and surface chemical compositions of polymer blends are not the same even though they are miscible in the bulk. For example, the surface of the blends of poly(vinyl alcohol) (PVAL) and poly(*N*-vinyl-2-pyrrolidone) is enriched with lower surface free energy component (PVAL) even though the components are miscible in the bulk [4]. However, it is possible to eliminate surface enrichment of the low energy component at the surface when the interaction between the components is strong. In the blends of poly(styrene-*co*-*p*-hexafluorohydroxyisopropyl-α-methyl styrene)/poly(4-vinyl pyridine) (PS(OH)/PVPy), the interaction between the two components could be controlled by changing the density of hydrogen bonding through the adjustment of the hydroxyl content of the PS(OH) component [5]. When the hydroxyl content was lower than 5 mol%, the surface of these polymer blends was largely enriched with PS(OH) because of the difference in surface free energy between PS(OH) and PVPy. When the hydroxyl content was higher than 21 mol%, complexes formed rendering the surface and bulk compositions very similar.

Time-of-flight secondary ion mass spectrometry (ToF-SIMS) and atomic force microscopy (AFM) are two surface

* Corresponding authors. Tel./fax: +852-2358-7125.
E-mail addresses: kecmchan@ust.hk (C.M. Chan), lilin@infoc3.icas.ac.cn; Tel: +10-82619830; Fax: +10-62559373 (L. Li).

0032-3861/03/$ - see front matter © 2003 Elsevier Science Ltd. All rights reserved.
doi:10.1016/S0032-3861(03)00328-8

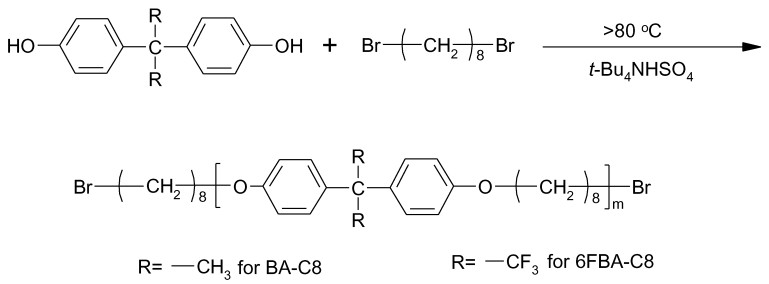

Scheme 1. Synthesis of BA-C8 and 6FBA-C8.

analysis techniques that have been shown to be invaluable as tools for polymer surface investigations. ToF-SIMS has been widely used to study polymer surface structures, including chain end groups [6], pendant groups [7], repeat units, chain conformations, crosslinking, branching, segmental distributions [8] and polymer chain interaction [4,9]. More recently, ToF-SIMS imaging has been used to investigate the surface morphologies of polymer blends such as PVC (Poly vinylchloride)/poly(methyl methacrylate) (PMMA) [10] and ethylene-tetrafluoroethylene copolymer and PMMA [11]. AFM has been a useful technique for acquiring topological information about surfaces. Recently, with the development of the tapping-mode AFM (TM-AFM), both height and phase images can be obtained at the same time, providing the information on the surface morphology of the polymer blends [12–15]. The combination of these two techniques is proving invaluable to the study of polymers [16–23].

In this work, two polymers—BA-C8 and 6FBA-C8—were synthesized. BA-C8 and 6FBA-C8 are semi-crystalline and amorphous polymers, respectively. We anticipated that this blend is miscible because they have similar chemical structures. A blend of BA-C8/6FBA-C8 with a weight ratio of BA-C8 to 6FBA-C8 of four was prepared and the changes in the chemical and morphological properties of the blend surface as the BA-C8 polymer crystallized were studied using contact angle measurements, ToF-SIMS and AFM. The surface chemical composition of the blend as a function of time was studied using X-ray photoelectron spectroscopy (XPS). The results suggested a mechanism for the observed surface chemical and morphological development.

Table 1
Characteristics of the polymers and blends

Sample	T_g (°C)	T_m (°C)	$\overline{M}_w \times 10^3$ (g mol^{-1})	$\overline{M}_w/\overline{M}_n$
BA-C8-1	6.9	84.0	9.5	1.7
BA-C8-2	13.6	91.0	13.6	1.6
6FBA-C8	27.8		8.0	1.5
BA-C8-1/6FBA-C8(80:20)	9.8	82.5		
BA-C8-2/6FBA-C8(80:20)	15.2	84.0		

2. Experimental section

BA-C8 and 6FBA-C8 were obtained by condensation polymerization of 1,8-dibromo-octane with bisphenol-A and 4,4′-(hexafluoroisopropylidene)diphenol, respectively [24]. The syntheses are described in Scheme 1

The physical properties of the polymers are listed in Table 1. A mixture containing 80 wt% of BA-C8 and 20 wt% of 6FBA-C8 was dissolved in chloroform, resulting in a clear solution with the polymer concentration of 30 mg ml^{-1}. A film sample was prepared by the spin-casting method. About 40 μl of solution was cast at 4000 rpm on a 1 cm^2 silicon wafer. The film was dried in a vacuum oven for 30 min at room temperature. The thickness of the film was measured to be about 220 nm using a profilometer.

AFM height and phase images were collected with a NanoScope III™ AFM (Digital Instruments) at room temperature. The exact surface temperature was probably a little bit higher than the room temperature due to the heating of the laser. Si tips with a resonance frequency of ~300 kHz were used and the scan rate was 0.8 Hz. The set-point amplitude ratio was set at 0.8. For each image, 512 lines were collected.

ToF-SIMS measurements were performed on a Physical Electronics PHI 7200 ToF-SIMS spectrometer. The vacuum was about 1.5×10^{-9} Torr. High-resolution mass spectra were obtained using a Cs^+ primary ion source operating at 8 keV. The total ion dose was lower than 4×10^{11} ions cm^{-2}. Positive and negative spectra were taken. The chemical images were acquired in the negative mode using a $^{69}Ga^+$ liquid metal ion source operating at 25 keV. The mapped area was 100 μm × 100 μm with a maximum of 50 frame scans.

XPS spectra were recorded on a PHI 5600 multi-technique system equipped with an Al monochromatic X-ray source. A pass energy of 58.7 eV was used. The spectra were obtained at a take-off angle of 45°. The wt% of 6FBA (W_{6FBA}) at the surface was calculated using the following equation

$$W_{6FBA} = \frac{223R_{F/O}}{54R_{F/O} + 507} \quad (1)$$

where $R_{F/O}$ is the F-to-O atomic ratio.

Differential scanning calorimetry (DSC) measurements

Table 2
Surface energies for water and methylene iodide

Liquid	γ_l^p (mJ m^{-2})	γ_l^d (mJ m^{-2})	γ_l (mJ m^{-2})
Water	51.0	21.8	72.8
Methylene iodide	1.3	49.5	50.8

were performed with a TA 2910 calorimeter in a nitrogen atmosphere. The heating rate was 8 °C min^{-1} and the temperature ranged from −50 to 200 °C. Two heating and cooling cycles were used. The melting point (T_m) was taken from the first heating cycle, and the glass transition temperature (T_g) was taken from the second heating cycle.

Contact angles were measured on a Kruss goniometer at room temperature. The volume of the droplet was 15 μl. Contact angles were measured at different times after the films were prepared. Three films were used for the contact angle measurements to obtain an average value at a particular crystalline time. An average value was obtained from 5 to 7 measurements for each film sample. The surface energy was determined by using the Owens–Wendt method [25]. According to this method, the relationship between the contact angle, θ, and the surface energy of the liquid, γ_{lv}, can be written

$$1 + \cos\theta = 2\sqrt{\gamma_s^d}\left(\frac{\sqrt{\gamma_l^d}}{\gamma_{lv}}\right) + 2\sqrt{\gamma_s^p}\left(\frac{\sqrt{\gamma_l^p}}{\gamma_{lv}}\right) \quad (2)$$

where γ_s^d and γ_s^p are the dispersive and polar components of the surface energy of the solid, respectively, and γ_l^d and γ_l^p are the dispersive and polar components of the surface energy of the liquid, respectively. The surface energy of the solid is given by

$$\gamma_s = \gamma_s^d + \gamma_s^p \quad (3)$$

By measuring the contact angles of two different liquids with known surface energies, the surface energy of the solid can be obtained by solving Eq. (2). Water and methylene iodide were used and their surface energies are listed in Table 2.

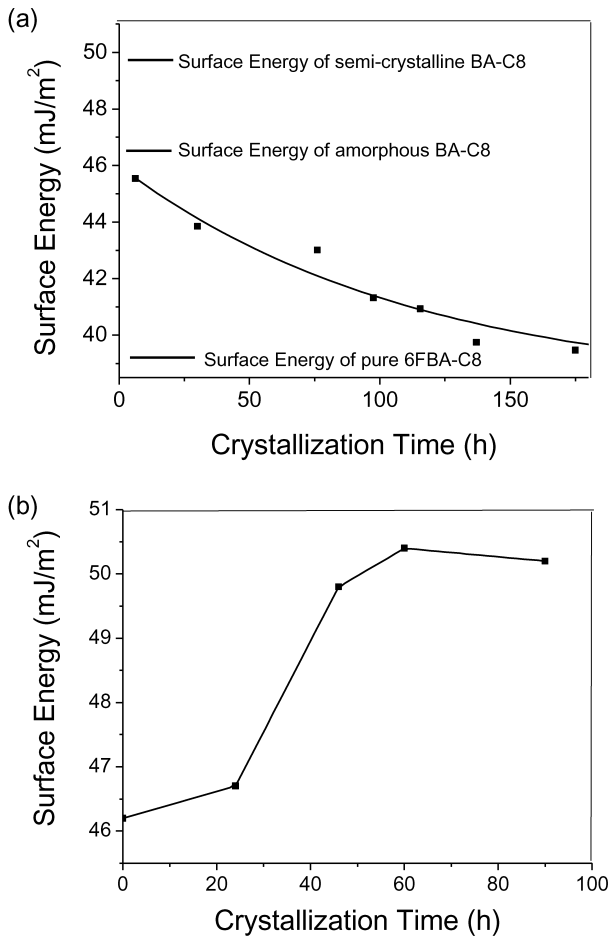

Fig. 1. (a) Plot of the surface energy of the BA-C8-2/6FBA-C8 (80/20) blend as a function of crystallization time. (b) Plot of surface energy of the BA-C8-2 as a function of crystallization time.

3. Results and discussions

The T_g and T_m of BA-C8-1, BA-C8-2 and 6FBA-C8 as well as the BA-C8-1/6FBA-C8(80/20) and BA-C8-2/6FBA-C8 blends are listed in Table 1. The T_m of the blends was slightly lower than that of pure BA-C8. It is generally accepted that a polymer blend is miscible if only one T_g, which lies between those of the two pure polymers, is detected [26–29]. The BA-C8-1/6FBA-C8(80/20) and BA-C8-2/6FBA-C8(80/20) blends were determined to have a single T_g at 9.8 and 13.0 °C, respectively. The $T_{g,blend}$ of a miscible blend can be predicted by using the Fox equation [30].

$$\frac{1}{T_{g,blend}} = \frac{w_1}{T_{g1}} + \frac{w_2}{T_{g2}} \quad (4)$$

where w_1 and T_{g1} are the weight fraction and the glass transition temperature of component 1, respectively. Using this equation, the predicted $T_{g,blend}$ is 9.8 and 15.2 °C for the BA-C8-1/6FBA-C8(80/20) and BA-C8-2/6FBA-C8(80/20) blends, respectively, which are fairly close to the experimentally determined values. The DSC results indicate that the BA-C8-1/6FBA-C8(80/20) and BA-C8-2/6FBA-C8(80/20) blends are miscible at the weight ratio of 80/20.

Fig. 1(a) shows the surface energy of the BA-C8-2/6FBA-C8(80/20) blend as a function of time. The surface energy of a freshly prepared blend sample was measured to be about 45.5 mJ m^{-2} which is slightly lower than that of a pure amorphous BA-C8 film (46.5 mJ m^{-2}). A gradual decrease in surface energy was observed as 6FBA migrated to the surface and finally reached a steady value of about 39.5 Nm m^{-1}, which is very similar to that of pure 6FBA-C8 (39.4 mJ m^{-2}), after 200 h. These results indicate that the surface of the blend consisted of mostly 6FBA-C8. It is

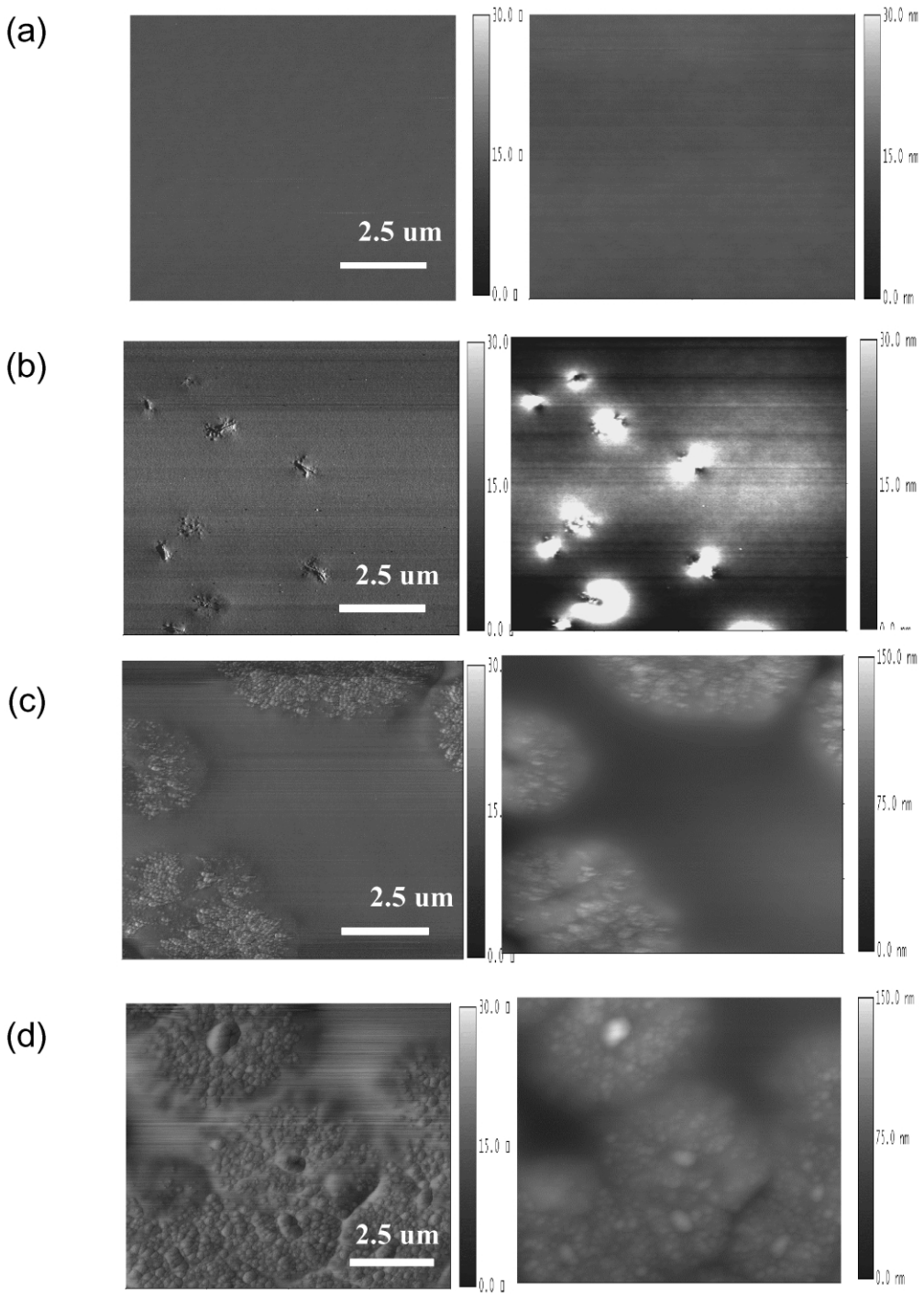

Fig. 2. AFM height (right column) and corresponding phase images (left column) for the BA-C8-2/6FBA-C8 (80/20) blend with time (a) 1 h, (b) 60 h, (c) 140 h and (d) 200 h after the sample was prepared.

clear that the contact angle data suggest that the surface composition of the film changed during crystallization.

Fig. 1(b) shows the change in the surface energy of an amorphous BA-C8-2 film as it crystallized. The surface energy increased from 46.5 mJ m^{-2} for an amorphous BA-C8-2 film to about 50 mJ m^{-2} for a semi-crystalline film. The increase in the surface energy of BA-C8 as it crystallizes would increase the thermodynamic driving force for the migration of the low surface energy component of the blend.

The crystallization of the BA-C8-2/6FBA-C8(80/20) blend was studied with AFM. Fig. 2 shows the TM-AFM height images (right column) and corresponding phase images (left column) for the blend at different times: (a) 1 h, (b) 60 h, (c) 140 h, and (d) 200 h after the sample was prepared. The height and phase are quite uniform across the

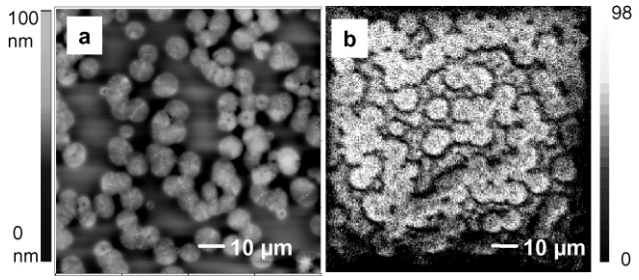

Fig. 3. AFM height image (a) and the corresponding ToF-SIMS F^- image (b) for the BA-C8-1/6FBA-C8 (80/20) blend 68 h after it was prepared.

scanned area (100 μm^2), indicating that the surface of the blend is homogeneous. According to previously published results [31], if crystallization had occurred, the surface of the crystalline regions would be lower than the level of the amorphous regions. Hence, we can conclude that the blend was amorphous after 1 h. As shown in Fig. 2(b), lamellar sheafs appeared on the surface after 60 h. However, on the blend surface, we cannot see the individual lamellae of BA-C8 as clearly as what we can see on the film of a pure BA-C8 sample because the surface of the blend was covered with a layer of 6FBA-C8. Fig. 2(c) shows the lamellar sheafs grew and became small spherulites with diameters of about 3 to 4 μm after 140 h. After 200 h, spherulites with diameters large than 5 μm impinged each other. A careful examination of the phase and height images, as shown in Fig. 2(d), reveals that many small disc-like features on the surface of the spherulites due to the inclusion of the noncrystallizable component in the spherulites. The boundaries between the discs, as observed in the images, are believed to be the regions where 6FBA-C8 accumulated within the spherulites underneath the 6FBA-C8 layer.

The crystallization rate of the blend was much slower than that of the pure BA-C8 polymer. For the pure polymer, nucleation was observed 2 h after it was prepared and the surface was fully covered with 20-μm spherulites within 24 h [31]. Factors which may have contributed to the slow crystallization rate of the BA-C8 polymer in the blend include (1) the decrease in the concentration of the BA-C8 polymer at the lamellar growth front; (2) the presence of the high T_g polymer (6FBA-C8) decreasing the mobility of the polymer chains of the crystalline component (BA-C8) and (3) the decreased *Tm* of the BA-C8 polymer in the blend decreasing the degree of undercooling [26].

In general, the crystalline regions have a higher density than that of the amorphous regions; hence, shrinkage occurred at regions where crystallization had occurred. The observation that the crystalline regions were much higher than the surrounding amorphous areas are contrary to

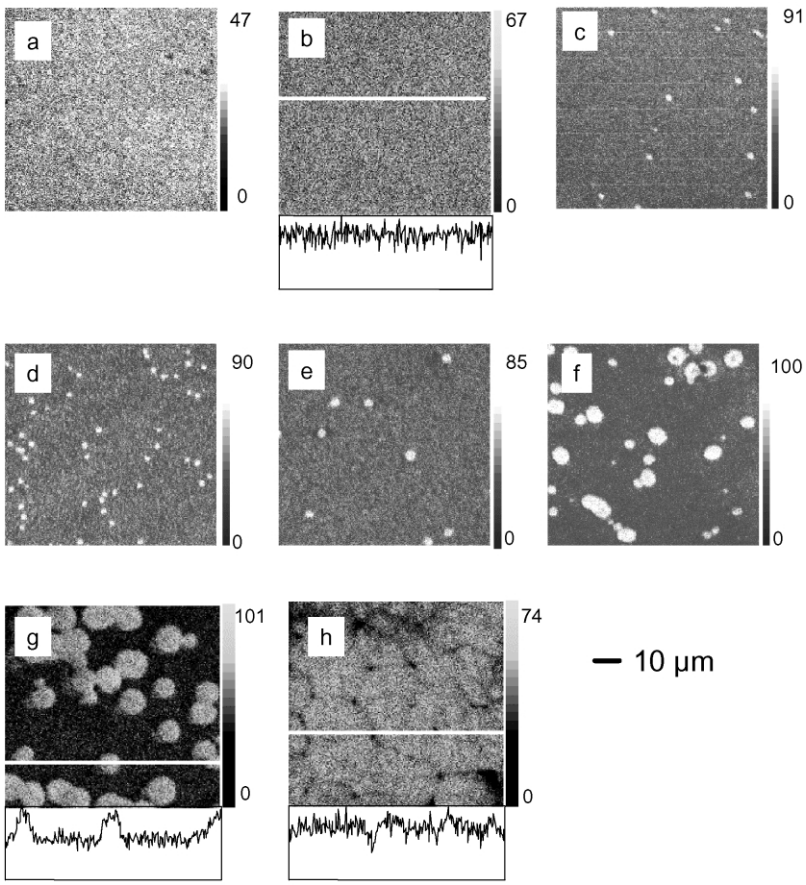

Fig. 4. F^- images of the surface of the BA-C8-1/6FBA-C8(80/20) blend with time: (a) 1 h, (b) 6 h, (c) 12 h, (d) 22 h, (e) 36 h, (f) 48 h, (g) 68 h, and (h) 9 days after it was prepared.

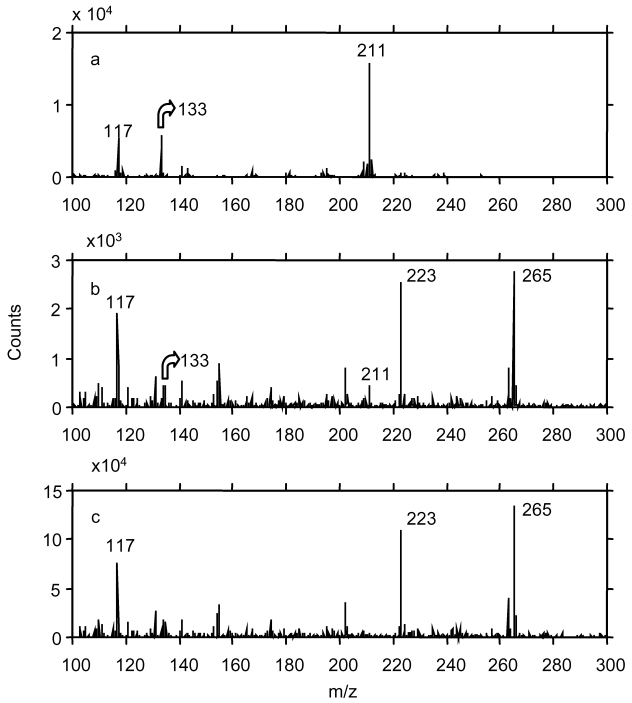

Fig. 5. Negative spectra with mass range of 100–300 amu for (a) the pure BA-C8-1 polymer (b) the BA-C8-1/6FBA-C8 (80/20) blend at 48 h after it was prepared and (c) the pure 6FBA-C8 polymer.

what has been observed for the pure BA-C8 polymer [31]. The spherulitic regions in Fig. 2(c) and (d) are about 150 nm higher than the surrounding amorphous regions. This can be explained by the difference in the mobility between the BA-C8 and 6FBA-C8 polymers. When BA-C8 crystallizes in the blend, the BA-C8 chains migrate from the surrounding amorphous regions to the lamellar growth front and fold into the crystal lattice during crystallization. However, the mobility of the 6FBA-C8 chains is fairly limited at room temperature because its T_g, is 27.8 °C, which is much higher than that of BA-C8. Although it is known that the mobility of the polymer chains at the surface is determined by the surface T_g, which is much lower than the bulk T_g [32]. We believe that the argument using the bulk T_gs is still valid because it is logical to assume that the surface T_g of 6FBA-C8 is much higher than that of BA-C8. Consequently, material flows into the crystalline regions. Another factor that causes the rise in the crystalline regions is that 6FBA-C8 tends to segregate at the surface of the crystalline regions because the surface energy of 6FBA-C8 is lower than that of BA-C8 due to the presence of two CF_3 groups in 6FBA-C8. Our contact angle results show that the surface energy of the crystalline phase of BA-C8 is much higher than its amorphous phase. Hence, the driving force for 6FBA-C8 to segregate to the surface increases as BA-C8 crystallizes.

The development of the surface morphology of the BA-C8-1/6FBA-C8(80/20) blend was also investigated with ToF-SIMS chemical imaging. The F^- images of the blend surface can be used to determine the spatial distribution of the BA-C8-1/6FBA-C8(80/20) blend components because the F^- is one of the negative characteristic ions of the 6FBA-C8 polymer and is absent from the BA-C8 polymer. Fig. 3(a) and (b) show the AFM height and F^- images, respectively, for the BA-C8-1/6FBA-C8(80/20) blend 68 h after it was prepared. The image size is 100 μm × 100 μm. As discussed previously, the higher regions in the AFM height image are the spherulites of the BA-C8 polymer. Examining the size and the distribution of the bright dots clearly shows that AFM and F^- images produced comparable results. Therefore, the regions which show a high fluorine intensity are the crystalline regions. Hence, the F^- images can be used to study the development of spherulites at the surface of the blend.

Fig. 4 displays ToF-SIMS F^- images for the BA-C8-1/6FBA-C8(80/20) blend at different times after it was prepared. After 6 h, as shown in Fig. 4(b), the fluorine concentration was still quite uniform across the surface, indicating that no crystalline regions had formed. Bright spots (crystalline regions), representing areas of high fluorine concentration, of size of approximately 2 μm were seen at the surface after 12 h (see Fig. 4(c)). The size of the spherulites increased with time, as shown in Fig. 4(d)–(h). When the spherulites impinged each other, as shown in Fig. 4(h), the surface chemical composition became relatively uniform again. The whole surface of the sample was covered mostly by 6FBA-C8. It is important to point out that when comparing between the results shown in Figs. 2 and 4, we have to keep in mind that the crystallization rate of the BA-C8-1/6FBA-C8(80/20) blend is faster than that of BA-C8-2/6FBA-C8(80/20) because the molecular weight of BA-C8-1 is lower than that of BA-C8-2.

The distribution of 6FBA-C8 at the surface of the BA-C8-1/6FBA-C8(80/20) blend was also studied using line scans across the images, as shown in Fig. 4(b), (g) and (h). The line scan results, showing the F concentration along the line marked in the images, are displayed at the lower part of each image. Again the line scans, as depicted in Fig. 4(b), show that the fluorine concentration was indeed quite uniform across the sample 6 h after the sample was prepared, indicating that no crystalline regions had formed. The line scan, as shown in Fig. 4(g), reveals that spherulites of sizes varying from 10 to 15 μm had developed after 68 h. After 9 days, the surface was fully occupied by spherulites, as shown in Fig. 4(h). The fluorine concentration across the surface of each spherulite was quite uniform. At the boundary regions between the spherulites, a lower fluorine concentration was detected. This result can easily be explained by the fact that the crystallinity at the boundary regions was lower [31]. A lower crystallinity region would undoubtedly be a region with less severe phase separation between the BA-C8 and 6FBA-C8 polymers. This would give rise to a higher concentration of BA-C8 at the boundary and a lower concentration of fluorine.

ToF-SIMS spectra have been used in the identification of polymers. Figs. 5 and 6 show the negative and positive

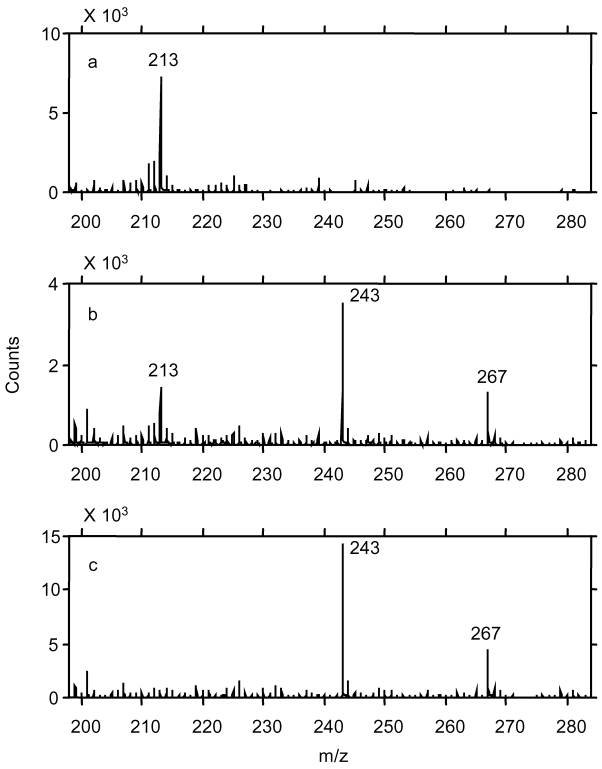

Fig. 6. Positive spectra with mass range of 200–300 amu for (a) the pure BA-C8-1 polymer (b) the BA-C8-1/6FBA-C8 (80/20) blend 48 h after it was prepared and (c) the pure 6FBA-C8 polymer.

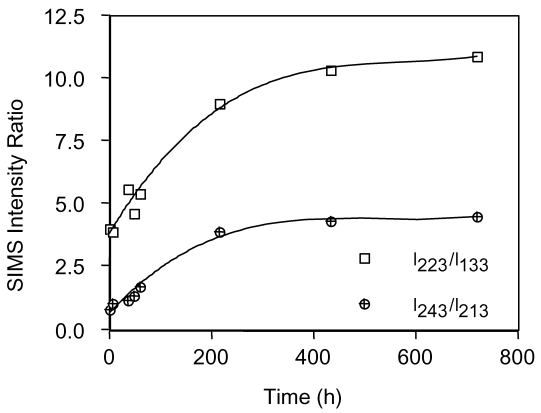

Fig. 7. The SIMS intensity ratios of some of the characteristic ions for the BA-C8-1/6FBA-C8 (80/20) blend as a function of time after it was prepared.

spectra, respectively, of the pure polymers and the BA-C8-1/6FBA-C8(80/20) blend. Characteristic positive and negative ions, as shown in Scheme 2, can be used to detect BA-C8 and 6FBA-C8 polymers. From the spectra of the blend, it is clear that ions characteristic of both BA-C8 and 6FBA-C8 are present. Hence, the ratio of the intensity of a characteristic ion of 6FBA-C8 to the intensity of a characteristic ion of BA-C8 can be used to monitor the migration of 6FBA-C8 at the surface of the blend. Fig. 7 shows such data. The increase in the value of the ratios as a function of time is a clear indication of the migration of 6FBA-C8 at the surface of the blend. In addition, the surface chemical composition of the blend was determined by XPS.

Positive ions

BA: m/z = 107, m/z = 135, m/z = 213

6FBA: m/z = 107, m/z = 243, m/z = 267

Negative ions

BA: m/z = 117, m/z = 133, m/z = 211

6FBA: m/z = 117, m/z = 223, m/z = 265

Scheme 2. Characteristic positive and negative ions of BA-C8 and 6FBA-C8.

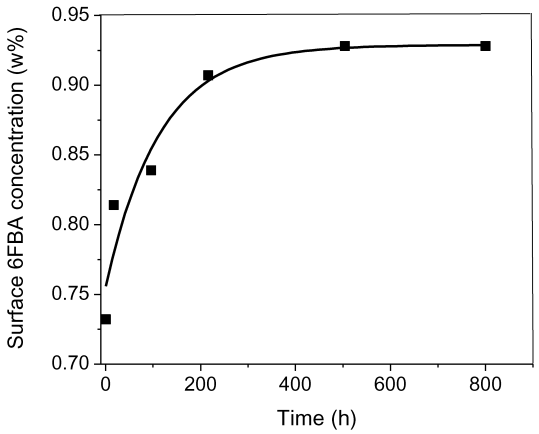

Fig. 8. The surface composition of the BA-C8-1/6FBA-C8(80/20) blend as a function of time after it was prepared.

Fig. 8 shows XPS results displaying the wt% of 6FBA at the surface of the BA-C8-1/6FBA-C8(80/20) blend as a function of time after the sample was prepared. Immediately after the sample was prepared, the surface concentration of 6FBA was about 73 wt%, which is substantially higher than the bulk value (20 wt%). After 800 h, the surface concentration of 6FBA increased to about 94 wt%. The ToF-SIMS and XPS results are consistent with the results from the contact angle measurements. However, it is important to point out that the sampling depths for contact angle measurements, ToF-SIMS and XPS are different. The surface composition revealed by these techniques would not be identical.

4. Conclusion

The BA-C8/6FBA-C8 blend was determined to be miscible by DSC. Even though the polymers are miscible in the bulk, surface segregation of the 6FBA-C8 polymer still occurred, especially at the crystalline regions, due to its lower surface energy. An additional driving force for 6FBA-C8 to segregate to the surface was provided by the crystallization of BA-C8. As BA-C8 crystallized, more BA-C8 migrated to the crystalline regions, causing the surface of the crystalline regions to rise above the amorphous regions. AFM, XPS and ToF-SIMS have been shown to be invaluable tools for studying the development of surface properties of polymer blends during crystallization.

Acknowledgements

This work was supported by the Hong Kong Grants Council under grant number HKUST6176/02 and the National Science Foundation of China and the Hong Kong Government Research Grants Council Joint Research Scheme under Grant No. N_HKUST 618/01 and the National Science Foundation China under grant number 20131160730.

References

[1] Chan CM. Polymer surface modification and characterization. New York: Hanser; 1994.
[2] Andrade JD. Polymer surface dynamics. New York: Plenum; 1988.
[3] Garbassi F, Morra M, Occhiello E. Polymer surfaces: from physics to technology. England: Wiley; 1994.
[4] Li L, Chan CM, Weng LT. Polymer 1998;39:2355.
[5] Liu S, Jiang M, Chan C-M, Weng LT. Macromolecules 2001;34:3802.
[6] Fowler DE, Johnson RD, Vanleyen D, Benninghoven A. Surf Interf Anal 1991;17:125.
[7] Castner DG, Ratner BD. Surf Interf Anal 1990;15:479.
[8] Zhuang HZ, Gardella Jr. JA, Hercules DM. Macromolecules 1997;30:1153.
[9] Li L, Chan CM, Weng LT, Xiang M, Jiang M. Macromolecules 1998;31:7248.
[10] Briggs D, Fletcher IW, Reichlmaier S, Agulo-Sanchez JL, Short RD. Surf Interf Anal 1996;24:419.
[11] Weng LT, Smith TL, Feng JY, Chan CM. Macromolecules 1998;31:928.
[12] Roberts CJ, Williams PM, Davies MC, Jackson DE, Tendler SJB. Trends Biotechnol 1994;12:127.
[13] Leggett GL, Davies MC, Jackson DE, Roberts CJ, Tendler SJB. Trends Polym Sci 1993;1:115.
[14] Drake B, Prater CB, Weisenhorn AL, Gould SAC, Albrecht TR, Quate CF, Cannell DS, Hansma HG, Hansma PK. Science 1989;243:1586.
[15] Marti O, Ribi HO, Drake B, Albrecht TR, Quate CF, Hansma PK. Science 1988;239:50.
[16] Shakeseff KM, Chen XY, Davies MC. Abstr Pap Am Chem S 209: 28-Poly, Part 2; 2 Apr 1995.
[17] Shakeseff KM, Davies MC, Heller J. Langmuir 1995;11:2547.
[18] Davies MC, Shakesheff KM, Shard AG. Macromolecules 1996;29:2205.
[19] Leadley SR, Shakesheff KM, Davies MC. Biomaterials 1998;19:1353.
[20] Karim A, Slawecki TM, Kumar SK. Macromolecules 1998;31:857.
[21] Xu KY, Gusev AI, Hercules. Surf Interf Anal 1999;27:659.
[22] Yuan YM, Shoichet MS. Macromolecules 2000;33:4926.
[23] Lammertink RGH, Hempenius MA, Vancso GJ. Macromolecules 2001;34:942.
[24] Li L, Chan CM, Ng KM, Lei YG, Weng LT. Polymer 2001;42:6841.
[25] Owens DK, Wendt RC. J Appl Polym Sci 1969;13:1741.
[26] Xing PX, Dong LS, An YX, Feng ZL, Avella M, Martuscelli E. Macromolecules 1997;30:2726.
[27] Avella M, Martuscelli E. Polymer 1988;29:1731.
[28] Avella M, Greco P, Martuscelli E. Polymer 1991;32:1647.
[29] Avella M, Martuscelli E, Raimo M. Polymer 1993;34:3234.
[30] Fox TG. Bull Am Phys Soc 1956;1:123.
[31] Li L, Chan CM, Yeung KL, Li JX, Ng KM, Lei YG. Macromolecules 2001;34:316.
[32] Kajiyama K, Tanak K, Takahara A. Macromolecules 1997;30:6626.